

Localization-Based Beam Focusing in Near-Field Communications

Nima Mozaffarikhosravi, Prathapasinghe Dharmawansa, and Italo Atzeni

Abstract—Shifting 6G-and-beyond wireless communication systems to higher frequency bands and the utilization of massive multiple-input multiple-output arrays will extend the near-field region, affecting beamforming and user localization schemes. In this paper, we propose a localization-based beam-focusing strategy that leverages the dominant line-of-sight (LoS) propagation arising at mmWave and sub-THz frequencies. To support this approach, we analyze the 2D-MUSIC algorithm for distance estimation by examining its spectrum in simplified, tractable setups with minimal numbers of antennas and users. Lastly, we compare the proposed localization-based beam focusing, with locations estimated via 2D-MUSIC, with zero forcing with pilot-based channel estimation in terms of uplink sum spectral efficiency. Our numerical results show that the proposed method becomes more effective under LoS-dominated propagation, short coherence blocks, and strong noise power arising at high carrier frequencies and with large bandwidths.

Index Terms—2D-MUSIC algorithm, beam focusing, localization, near-field communications.

I. INTRODUCTION

The development of 6G-and-beyond wireless networks, driven by emerging applications such as holographic communications and high-precision sensing, is expected to introduce new bandwidth demands [1]. A promising way to accommodate this growth is to shift operations toward higher frequency bands, including the mmWave and sub-THz ranges [2]. As the carrier frequency increases, massive multiple-input multiple-output (MIMO) arrays are needed to overcome the challenging propagation; at the same time, antennas become physically smaller, thus facilitating the deployment of compact massive MIMO arrays [3]. When operating with large arrays at smaller wavelengths, the radiative near-field region extends significantly, impacting both beamforming (or beam focusing) and user localization schemes [4]. The near-field spherical wavefronts can be leveraged to focus the signals on precise spatial locations, which allows to perform user localization by estimating both distance and angle with a single base station (BS). In addition, due to increased pathloss and scattering absorption at mmWave and sub-THz frequencies, non-line-of-sight (NLoS) paths become less impactful and the channel is typically dominated by line-of-sight (LoS) components [5]. Thus, it becomes more practical to exploit user localization methods for beam-focusing design, as the comparatively lower signaling overhead of localization algorithms can help enhance the system's spectral efficiency (SE) [6], [7].

The work in [8] compares far-field and near-field user localization, reviewing different aspects of the localization procedure and the most common algorithms used in the literature. Moreover, [9] examines the challenges of user localization and channel estimation in the near field, and provides a survey of relevant algorithms. The study in [10] analyzes the two-dimensional multiple signal classification (2D-MUSIC) algorithm for parametric near-field channel estimation in multi-user MIMO systems, deriving a closed-form Cramér-Rao bound and demonstrating that 2D-MUSIC achieves near-optimal performance compared to non-parametric and sequential alternatives. Furthermore, [11] proposes a modification of the 2D-MUSIC algorithm that reduces the complexity of the search procedure, therefore facilitating its application in localization-based near-field communication systems. In [12], a near-field localization approach is presented for a hybrid analog-digital receiver equipped with a dynamic metasurface antenna and 1-bit analog-to-digital converters. While prior works have investigated near-field localization and channel estimation, the explicit use of localization for beam-focusing design, particularly leveraging the LoS-dominated propagation at high frequencies, remains unaddressed.

In this paper, we provide the following contributions. First, we consider a near-field channel model with LoS and NLoS propagation and add a frequency-dependent scattering reflection coefficient that accounts for the LoS-dominated propagation at high carrier frequencies, utilizing a function based on real measurement data in our simulations. Then, we propose a localization-based beam-focusing design, which leverages the LoS-dominated propagation at mmWave and sub-THz frequencies. To support this approach, we analyze the 2D-MUSIC algorithm for distance estimation by examining its spectrum in simplified, tractable setups with minimal numbers of antennas and users. These configurations enable closed-form analysis and offer deeper insights into the distance estimation error and the impact of interference. Lastly, we compare the proposed localization-based beam focusing, with locations estimated via 2D-MUSIC, with zero forcing (ZF) with pilot-based channel estimation in terms of uplink (UL) sum spectral efficiency (sum-SE). Our numerical results show that, despite the added offline complexity of the 2D-MUSIC algorithm, the proposed method becomes more effective under LoS-dominated propagation, short coherence blocks, and strong noise power arising at high carrier frequencies and with large bandwidths.

II. SYSTEM AND CHANNEL MODEL

In this section, we introduce the considered system model and near-field channel model with LoS and NLoS propagation and frequency-dependent reflection.

The authors are with the Centre for Wireless Communications, University of Oulu, Finland (e-mail: {nima.mozaffari, prathapasinghe.kaluwadevage, italo.atzeni}@oulu.fi). This work was supported by the Research Council of Finland (336449 Profi6, 348396 HIGH-6G, and 369116 6G Flagship).

A. System Model

Consider a MIMO system where K single-antenna users are served by a BS with N antennas in the UL. The received data signal at the BS is given by

$$\mathbf{y} = \sum_{k=1}^K \sqrt{\rho_k} \mathbf{h}_k s_k + \mathbf{n} \in \mathbb{C}^{N \times 1}, \quad (1)$$

where ρ_k represents the transmit power of user k , $\mathbf{h}_k \in \mathbb{C}^{N \times 1}$ is the random channel between user k and the BS, $s_k \in \mathbb{C}$ denotes the data symbol of user k satisfying $\mathbb{E}[|s_k|^2] = 1$ and $\mathbb{E}[s_k s_i^*] = 0$, $\forall i \neq k$, and $\mathbf{n} \sim \mathcal{CN}(\mathbf{0}, \sigma^2 \mathbf{I}_N)$ is a vector of additive white Gaussian noise (AWGN). The channel characteristics depend on the users' distance from the BS and whether they are located in the near or far field of the BS, as discussed in Section II-B.

Channel estimation in time-division duplex is typically carried out via UL pilots, transmitted simultaneously by all the users. Let $\mathbf{p}_k \in \mathbb{C}^{\tau_{\text{pil}} \times 1}$ denote the pilot of user k , where τ_{pil} is the pilot length. Assuming $\tau_{\text{pil}} \geq K$, we consider orthogonal pilots such that $\mathbf{p}_k^H \mathbf{p}_i = 0$, $\forall i \neq k$. Furthermore, we assume that each entry of \mathbf{p}_k has unit magnitude to ensure a constant power level. The received pilot signal at the BS is given by

$$\mathbf{Y}_{\text{Pil}} = \sum_{k=1}^K \sqrt{\rho_k} \mathbf{h}_k \mathbf{p}_k^T + \mathbf{N}_{\text{Pil}} \in \mathbb{C}^{N \times \tau_{\text{pil}}}, \quad (2)$$

where $\mathbf{N}_{\text{Pil}} \in \mathbb{C}^{N \times \tau_{\text{pil}}}$ is a matrix of AWGN with independent and identically distributed (i.i.d.) $\mathcal{CN}(0, \sigma^2)$ entries. The channel estimate is then obtained from (2) using, for example, the least-squares (LS) estimator

$$\hat{\mathbf{h}}_k = \frac{1}{\sqrt{\rho_k \tau_{\text{pil}}}} \mathbf{Y}_{\text{Pil}} \mathbf{p}_k^* \in \mathbb{C}^{N \times 1}, \quad (3)$$

which does not require any statistical knowledge about the channel and is considered as part of our baseline in Section IV.

Let $\mathbf{w}_k \in \mathbb{C}^{N \times 1}$ denote the receive combiner corresponding to user k . The resulting signal-to-interference-plus-noise ratio (SINR) of user k is given by

$$\text{SINR}_k = \frac{\rho_k |\mathbf{w}_k^H \hat{\mathbf{h}}_k|^2}{\sum_{i \neq k} \rho_i |\mathbf{w}_k^H \hat{\mathbf{h}}_i|^2 + \sigma^2 \|\mathbf{w}_k\|^2}. \quad (4)$$

Finally, the UL sum-SE of the system can be expressed as $\text{sum-SE} = (1 - \frac{\tau_{\text{pil}}}{T}) \mathbb{E}[\sum_{k=1}^K \log_2(1 + \text{SINR}_k)]$ [bit/s/Hz], where T is the size of the coherence block and the expected value is with respect to the channel realizations. While the receive combiners are typically constructed based on the channel estimates, we propose an alternative localization-based receive combiner design in Section III, which turns out to be remarkably effective under LoS-dominated propagation.

B. Near-Field Channel Model

Assume that the BS is equipped with a uniform linear array (ULA) with antenna spacing d and total length $D = (N - 1)d$. Denote the carrier frequency as f_c and the corresponding wavelength as $\lambda_c = \frac{c}{f_c}$, where c is the speed of light. The Fraunhofer distance, which is commonly used to separate the near- and far-field regions, is defined as $R_F = \frac{2D^2}{\lambda_c}$. We assume

that the carrier frequency, the ULA length, and the distance of the users and scatterers from the BS are such that both the LoS and NLoS paths are subject to near-field propagation. For a source defined by the angle θ and distance r , the near-field steering vector is given by [13]

$$\mathbf{b}(f_c, r, \theta) = \begin{bmatrix} e^{-j \frac{2\pi}{\lambda_c} (\bar{r}_0(r, \theta) - r)} \\ \vdots \\ e^{-j \frac{2\pi}{\lambda_c} (\bar{r}_{N-1}(r, \theta) - r)} \end{bmatrix} = \begin{bmatrix} b_1 \\ \vdots \\ b_N \end{bmatrix} \in \mathbb{C}^{N \times 1}, \quad (5)$$

where

$$\bar{r}_n(r, \theta) = \sqrt{r^2 + \delta_n^2 d^2 - 2r\delta_n d \sin \theta} \quad (6)$$

denotes the distance from the n th antenna, with $\delta_n = \frac{2n - N + 1}{2}$, $\forall n = 0, \dots, N - 1$. For notational simplicity, we omit the dependence on r and θ in (6) in the following.

We consider a general near-field channel model with LoS and NLoS propagation, where the latter follows the clustered multipath model in [14, Ch. 5.6.1] with L NLoS paths. Each NLoS path originates from a cluster comprising a large number of scatterers, which contributes to the signal's random phase rotation and power fluctuation. Without loss of generality, we assume that the L clusters are common to all the users. Let $\theta_k \in [-\frac{\pi}{2}, \frac{\pi}{2}]$ and $\theta_\ell^{\text{NLoS}} \in [-\frac{\pi}{2}, \frac{\pi}{2}]$ denote the angles of user k and the ℓ th cluster, respectively, relative to the array's broadside direction. Furthermore, let r_k and r_ℓ^{NLoS} denote the distances from user k and the ℓ th cluster, respectively, to the center of the receiver. Considering a common pathloss factor for all the antennas as in [14, Ch. 5.6.1], the channel between the BS and user k is modeled as

$$\mathbf{h}_k = \underbrace{\frac{\lambda_c}{4\pi r_k} e^{-j \frac{2\pi}{\lambda_c} r_k} \mathbf{b}(f_c, r_k, \theta_k)}_{\text{LoS}} + \underbrace{\sum_{\ell=1}^L g_{k,\ell} \mathbf{b}(f_c, r_\ell^{\text{NLoS}}, \theta_\ell^{\text{NLoS}})}_{\text{NLoS}}, \quad (7)$$

where $g_{k,\ell}$ is the small-scale fading coefficient of user k 's ℓ th NLoS path. Note that, for the NLoS paths, we have ignored the first hop from the users to the clusters to avoid making assumptions about the clusters' geometry and relative distances of the users: this results in a slight overestimation of the power of the NLoS paths, which in turn underestimates the gains of the proposed localization-based beam focusing. Hence, we have $g_{k,\ell} \sim \mathcal{CN}(0, \gamma_\ell^2)$, $\forall k = 1, \dots, K$, where γ_ℓ^2 models the large-scale fading of the ℓ th NLoS path. In this paper, we introduce an additional frequency-dependent reflection coefficient, which is typically not included in existing works. Specifically, we define

$$\gamma_\ell^2 = \left(\frac{\lambda_c}{4\pi r_\ell^{\text{NLoS}}} \right)^2 \alpha_\ell(f_c), \quad (8)$$

where $\alpha_\ell(f_c) \in (0, 1]$ models the reflection at the ℓ th scatterer. This term captures the increased scattering absorption at higher frequencies and is thus a decreasing function of f_c . Notably, setting $\alpha_\ell(f_c) = 1$ recovers existing channel models (e.g., [13]) that assume perfect reflection. In Section IV, we utilize a function for $\alpha_\ell(f_c)$ based on real measurement data from [15].

III. LOCALIZATION-BASED BEAM FOCUSING

Motivated by the fact that the NLoS paths tend to become less impactful at higher frequencies due to the increased pathloss and scattering absorption, we propose a localization-based beam-focusing strategy that leverages LoS-dominated propagation. In the proposed approach, the receive combiners are obtained by replacing the estimated channels $\{\hat{\mathbf{h}}_k\}$ with $\{\mathbf{b}(\hat{r}_k, \hat{\theta}_k)\}$ in conventional beamforming structures, where \hat{r}_k and $\hat{\theta}_k$ are the estimated distance and angle, respectively, of user k . In this paper, we consider a ZF structure, so the receive combining matrix is given by

$$\mathbf{W} = [\mathbf{w}_1, \dots, \mathbf{w}_K] = \hat{\mathbf{B}}(\hat{\mathbf{B}}^H \hat{\mathbf{B}})^{-1} \in \mathbb{C}^{N \times K}, \quad (9)$$

with $\hat{\mathbf{B}} = [\mathbf{b}(\hat{r}_1, \hat{\theta}_1), \dots, \mathbf{b}(\hat{r}_K, \hat{\theta}_K)] \in \mathbb{C}^{N \times K}$. The effectiveness of localization-based beam focusing clearly depends on the localization accuracy in both the distance and angular domains. Next, we describe near-field user localization based on the 2D-MUSIC algorithm, specifically focusing on distance estimation.

The conventional 2D-MUSIC algorithm exploits the orthogonality of the signal and noise spaces to localize the user via a 2D grid search for distance and angle [16]. First, UL pilots similar to those in Section II-A are simultaneously transmitted by all the users. In this context, let $\mathbf{q}_k \in \mathbb{C}^{\tau_{\text{Loc}} \times 1}$ denote the localization pilot for user k , where τ_{Loc} is the pilot length. We note that τ_{Loc} is typically smaller than τ_{Pil} : this benefits the effective sum-SE, as shown in Section IV. The received localization pilot signal at the BS is given by (cf. (2))

$$\mathbf{Y}_{\text{Loc}} = \sum_{k=1}^K \sqrt{\rho_k} \mathbf{h}_k \mathbf{q}_k^T + \mathbf{N}_{\text{Loc}} \in \mathbb{C}^{N \times \tau_{\text{Loc}}}, \quad (10)$$

where $\mathbf{N}_{\text{Loc}} \in \mathbb{C}^{N \times \tau_{\text{Loc}}}$ is a matrix of AWGN with i.i.d. $\mathcal{CN}(0, \sigma^2)$ entries. Based on (10), the sample covariance matrix of the received signal is obtained as

$$\mathbf{R}_{\text{Loc}} = \frac{1}{\tau_{\text{Loc}}} \mathbf{Y}_{\text{Loc}} \mathbf{Y}_{\text{Loc}}^H \in \mathbb{C}^{N \times N}. \quad (11)$$

Then, the noise eigenvector matrix, denoted by $\mathbf{U}_n \in \mathbb{C}^{N \times (N-K)}$, is formed by collecting the eigenvectors of \mathbf{R}_{Loc} associated with the $(N-K)$ smallest eigenvalues. Hence, the spectrum of the 2D-MUSIC algorithm corresponding to the N antennas and K users is expressed as [16]

$$S(f_c, r, \theta) = \frac{1}{\mathbf{b}^H(f_c, r, \theta) \mathbf{U}_n \mathbf{U}_n^H \mathbf{b}(f_c, r, \theta)}. \quad (12)$$

Finally, (12) is evaluated for different values of (r, θ) , and the K highest peaks yield the estimated locations of the K users.

To further investigate the distinctive features of the 2D-MUSIC algorithm in terms of distance estimation error and impact of interference, we analyze its spectrum in simplified, tractable setups with minimal numbers of antennas and users. These configurations allow for closed-form analysis and offer deeper insight into the algorithm's behavior. Nevertheless, the resulting conclusions apply to more general scenarios, as confirmed by our numerical results. To enable an accurate characterization of the algorithm's performance in terms of distance estimation, we assume perfectly known angles in the remainder of this section.

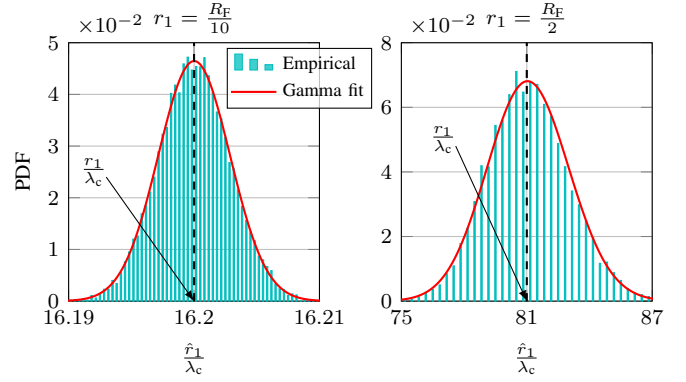


Fig. 1. Empirical PDF of the estimated distance based on (14), with $K = 1$, $N = 2$, $f_c = 100$ GHz, $\text{SNR} = 20$ dB, $\theta_1 = 0$ and $d = 9\lambda_c$.

A. Distance Estimation Error

To analyze the distance estimation error, we begin by considering a simplified setup with $K = 1$ and $N = 2$, which represents the simplest scenario that enables distance estimation with the 2D-MUSIC algorithm. For this setup with no interference, we can derive a closed-form expression for the estimated distance by maximizing (12) (i.e., minimizing its denominator). We begin by writing the denominator of (12) as

$$\begin{aligned} \frac{1}{S(f_c, r, \theta)} &= |u_1 b_1^* + u_2 b_2^*|^2 \\ &= |u_1|^2 + |u_2|^2 + 2|u_1||u_2| \\ &\quad \times \cos\left(\frac{2\pi}{\lambda_c}(\bar{r}_0 - \bar{r}_1) + \phi_1 - \phi_2\right), \end{aligned} \quad (13)$$

with $\mathbf{U}_n = [u_1 \ u_2]^T \in \mathbb{C}^{2 \times 1}$, $\bar{r}_0 = \sqrt{r^2 + \frac{d^2}{4} + rd \sin \theta}$, and $\bar{r}_1 = \sqrt{r^2 + \frac{d^2}{4} - rd \sin \theta}$, and where $\phi_k = \angle u_k$ denotes the phase of u_k , $k \in \{1, 2\}$. Now, we minimize (13) and obtain the estimated distance from

$$\hat{r}_1^2 = \frac{\frac{d^4}{4} - \kappa(\phi_1, \phi_2)^2}{4\kappa(\phi_1, \phi_2) - 2d^2 + 4d^2 \sin^2 \theta}, \quad (14)$$

with $\kappa(\phi_1, \phi_2) = \frac{d^2}{2} - \left(\frac{\lambda_c}{2\pi}((2M+1)\pi - \phi_1 + \phi_2)\right)^2$ and $M \in \mathbb{Z}$. However, the unique value of M , which directly affects the estimation accuracy, cannot be obtained analytically as (13) oscillates due to the presence of the cosine term, leading to multiple possible minimizing distances depending on the choice of M . Hence, M can only be determined by numerical analysis of the results around the true distance, assuming that a rough estimate of the true location is available.

Fig. 1 plots the empirical probability density function (PDF) of the estimated distance based on (14), with $f_c = 100$ GHz, $\text{SNR} = 20$ dB, $d = 9\lambda_c$, and $r_1 \in \{\frac{R_F}{10}, \frac{R_F}{2}\}$. Notably, the distance estimation error can be approximately modeled as a Gamma random variable. Accordingly, we have

$$\hat{r}_1 \simeq r_1 + \Delta r_1, \quad (15)$$

where $\Delta r_1 \sim \mathcal{G}(\mu, \nu)$ is the distance estimation error with variance $\zeta^2 = \mu\nu^2$. Although it is infeasible to analytically derive the statistical properties of Δr_1 (i.e., μ and ν) originating from the 2D-MUSIC algorithm, our simulation results reveal

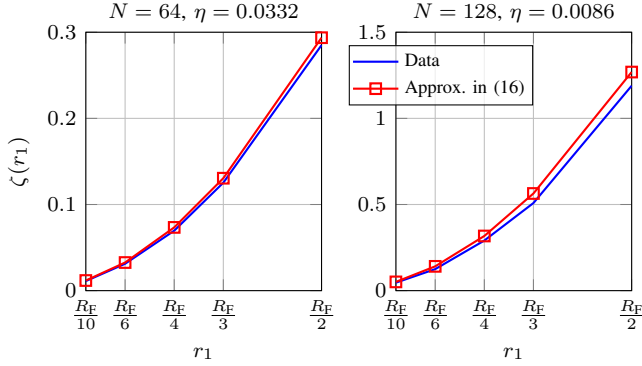


Fig. 2. Standard deviation of the distance estimation error versus distance, with $K=1$, $f_c=100$ GHz, SNR=20 dB, $\theta_1=0$ and $d=\frac{\lambda_c}{2}$.

that ζ^2 is closely related to the pathloss. Consequently, the variance of the distance estimation error for any distance in the near field can be approximated based on the numerically evaluated variance at a given distance. In this respect, Fig. 2 plots the standard deviation of the distance estimation error versus the estimated distance, with $K=1$, $N \in \{64, 128\}$, $f_c=100$ GHz, SNR=20 dB, and $d=\frac{\lambda_c}{2}$. It illustrates that the standard deviation scales quadratically with the distance and can be accurately approximated as

$$\zeta(r_1) \simeq \eta r_1^2, \quad (16)$$

where $\eta > 0$ needs to be numerically evaluated at a given distance. This scaling property turns out to be independent of both the number of antennas and their spacing.

B. Impact of Interference on the Distance Estimation

To analyze the impact of interference on the distance estimation, we consider a simplified setup with $K=2$ and $N=3$, which represents the simplest scenario encompassing interference in the 2D-MUSIC algorithm. We assume that the two users are aligned in the angular domain, i.e., $\theta_1 = \theta_2$. We begin by writing the denominator of (12) as

$$\begin{aligned} \frac{1}{S(f_c, r, \theta)} &= |u_1 b_1^* + u_2 b_2^* + u_3 b_3^*|^2 \\ &= 1 + 2|u_1||u_2| \cos\left(\frac{2\pi}{\lambda_c}(r - \bar{r}_0) + \phi_2 - \phi_1\right) \\ &\quad + 2|u_1||u_3| \cos\left(\frac{2\pi}{\lambda_c}(\bar{r}_2 - \bar{r}_0) + \phi_3 - \phi_1\right) \\ &\quad + 2|u_2||u_3| \cos\left(\frac{2\pi}{\lambda_c}(\bar{r}_2 - r) + \phi_3 - \phi_2\right), \quad (17) \end{aligned}$$

with $\mathbf{U}_n = [u_1 \ u_2 \ u_3]^T \in \mathbb{C}^{3 \times 1}$, $\bar{r}_0 = \sqrt{r^2 + d^2 + 2rd \sin \theta}$, $\bar{r}_2 = \sqrt{r^2 + d^2 - 2rd \sin \theta}$, and where $\phi_k = \angle u_k$ denotes the phase of u_k , $k \in \{1, 2, 3\}$. While straightforward closed-form expressions for \hat{r}_1 and \hat{r}_2 cannot be derived, the minima of (17) accurately estimate the distances of the two users for sufficiently high signal-to-noise ratio (SNR). Fig. 3 plots the denominator of the spectrum in (17) (evaluated numerically) versus the distance for different SNR values of user 1 (i.e., the closer user), with $f_c=100$ GHz, $d=9\lambda_c$, $r_1 = \frac{R_F}{4}$, and $r_2 = \frac{R_F}{2}$.¹ It

¹Here, we set $\sigma^2 = 1$ and normalize the channels with respect to the norm of the channel of user 1.

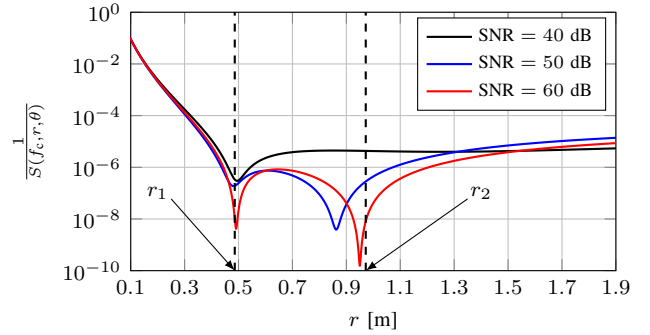


Fig. 3. Denominator of the spectrum versus distance, with $K=2$, $N=3$, $f_c=100$ GHz, $d=9\lambda_c$, $r_1 = \frac{R_F}{4}$, $r_2 = \frac{R_F}{2}$, and $\theta_1 = \theta_2 = 0$.

is observed that a relatively high SNR is required to accurately estimate the distance of user 2 (i.e., the farther user), since the spectrum is dominated by the signal of user 1 and the number of antennas is limited. For example, distance estimation for user 2 fails with SNR=40 dB, whereas increasing the SNR to 50 dB and 60 dB yields increasingly accurate estimates. Finally, increasing the number of antennas at the BS alleviates the need for high SNR, as it enhances spatial resolution and improves the separability of the users' signals.

IV. SUM-SE EVALUATION

In this section, we evaluate the UL sum-SE performance of the proposed localization-based beam focusing in the near field, examining the impact of key parameters such as the SNR and carrier frequency. The results illustrate the advantages of employing the receive combiner in (9) over conventional ZF with pilot-based channel estimation. While in Sections III-A and III-B we focused on distance estimation, in the following we adopt the 2D-MUSIC algorithm to estimate both the distances and angles of the users.

We consider a BS equipped with a ULA comprising $N=512$ antennas with spacing $d=\frac{\lambda_c}{2}$. $K=2$ users transmitting with equal power, i.e., $\rho_1 = \rho_2$, are located at distances $r_1 = \frac{R_F}{8}$ and $r_2 = \frac{R_F}{2}$ (with $R_F \simeq 392$ m at $f_c=100$ GHz) and angles $\theta_1 = \theta_2 = 0^\circ$ (i.e., aligned along the broadside direction of the ULA). In addition to the LoS path, we assume $L=2$ clusters of scatterers randomly located between the BS and the users. Without loss of generality, the NLoS paths are subject to the same reflection coefficient derived from linear fitting of the real measurement data in [15] (Mortar A, corresponding to a rough material), which yields $\alpha_l(f_c) = -0.0094(\frac{f_c}{10^9}) - 8.18$ dB. The size of the coherence block is set to $T=5000$ at $f_c=100$ GHz, which can accommodate a coherence bandwidth of 100 MHz and a user speed of 15 m/s. Moreover, T scales proportionally with λ_c as per [3, Rem. 2.1]. For pilot-based channel estimation, we adopt the LS estimator with pilot length $\tau_{\text{Pil}} = 0.2T$, which offers the best trade-off between channel estimation accuracy and pre-log factor of the sum-SE based on our simulations. For user localization via the 2D-MUSIC algorithm, we assume distance and angle steps $r_{\text{step}} \in \{10\lambda_c, 100\lambda_c\}$ and $\theta_{\text{step}} = 0.5^\circ$, respectively, and a pilot length of $\tau_{\text{Loc}} = 0.005T$. The AWGN power is modeled as $\sigma^2 = \xi - 174 + 10 \log_{10}(B)$ [dBm], where $\xi =$

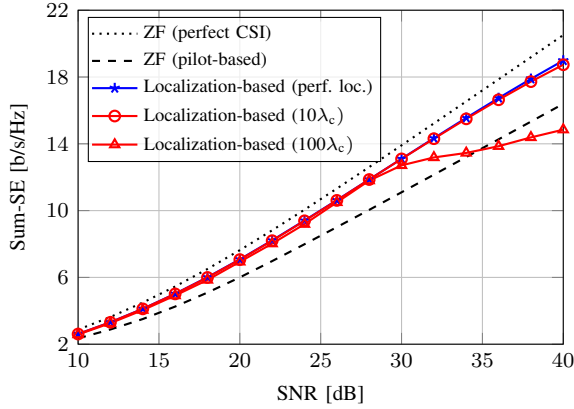


Fig. 4. Sum-SE versus SNR of user 1 with $K = 2$, $N = 512$, $f_c = 100$ GHz, $d = \frac{\lambda_c}{2}$, $r_1 = \frac{R_E}{8}$, and $r_2 = \frac{R_E}{2}$.

13 dB is the noise figure and B denotes the communication bandwidth, which is set to match the coherence bandwidth (e.g., $B = 100$ MHz at $f_c = 100$ GHz). The plots are obtained by averaging over 100 channel realizations, each generated by randomly moving the users within a radius of $10\lambda_c$ around their locations.

Fig. 4 plots the sum-SE as a function of the SNR of user 1 (i.e., the closer user)² at $f_c = 100$ GHz. The proposed localization-based beam focusing with distance resolution $r_{\text{step}} = 100\lambda_c$ outperforms ZF with pilot-based channel estimation, except at very high SNR (e.g., over 35 dB). Furthermore, by increasing the distance resolution to $r_{\text{step}} = 10\lambda_c$, our method achieves a sum-SE close to that obtained with (9) with perfect localization, which in turn approaches the performance of ZF with perfect channel state information (CSI). Fig. 5 illustrates the impact of the carrier frequency on the sum-SE. As the frequency grows, the proposed localization-based beam focusing becomes more robust to the decreasing coherence block and increasing AWGN power. Specifically, when T (and thus τ_{pil}) decreases and σ^2 increase, the accuracy of pilot-based channel estimation deteriorates, whereas localization-based beam focusing suffers less significantly from the reduced τ_{loc} and stronger AWGN. This suggests that, despite the added offline complexity, beam-focusing design based on user localization is a viable alternative to pilot-based methods in LoS-dominated mmWave and sub-THz systems.

V. CONCLUSION

In this work, we proposed a localization-based beam-focusing strategy for near-field communications leveraging LoS-dominated propagation, demonstrating the performance gains achieved by increasing the carrier frequency and varying the resolution of the localization algorithm. We also analyzed the 2D-MUSIC algorithm in terms of distance estimation error and impact of interference. Our numerical results showed that the proposed method outperforms ZF with pilot-based channel estimation in terms of UL sum-SE, except at very

²We set $\sigma^2 = 1$ and normalize the channels with respect to the norm of the channel of user 1.

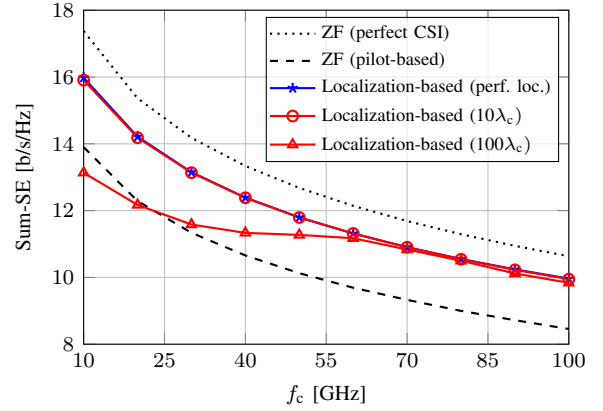


Fig. 5. Sum-SE versus carrier frequency with $K = 2$, $N = 512$, $\rho_1 = \rho_2 = 23$ dBm, $d = \frac{\lambda_c}{2}$, $r_1 = \frac{R_E}{8}$, and $r_2 = \frac{R_E}{2}$.

high SNRs. In this respect, user localization algorithms become more accurate as the frequency grows, showing great potential to enable precise beam focusing. Future work will investigate localization-based beam focusing utilizing more computationally efficient user localization algorithms along with optimized receive combiner design.

REFERENCES

- [1] N. Rajatheva *et al.*, “White paper on broadband connectivity in 6G,” <http://jultika.oulu.fi/files/isbn9789526226798.pdf>, 2020.
- [2] A. Singh *et al.*, “Near-field terahertz communications for 6G and beyond: From concepts to realizations,” *IEEE Signal Process. Mag.*, vol. 42, no. 1, pp. 106–125, 2025.
- [3] E. Björnson *et al.*, “Massive MIMO networks: Spectral, energy, and hardware efficiency,” *Found. and Trends Signal Process.*, vol. 11, no. 3–4, pp. 154–655, 2017.
- [4] D. Bodet *et al.*, “Sub-terahertz near field channel measurements and analysis with beamforming and Bessel beams,” *Sci. Rep.*, vol. 14, no. 1, p. 19675, 2024.
- [5] Y. Liu *et al.*, “Near-field communications: A comprehensive survey,” *IEEE Commun. Surveys and Tuts.*, pp. 1–1, 2024.
- [6] Z. Wang *et al.*, “Near-field localization and sensing with large-aperture arrays: From signal modeling to processing,” *IEEE Signal Process. Mag.*, vol. 42, no. 1, pp. 74–87, 2025.
- [7] D. Dardari and N. Decarli, “Holographic communication using intelligent surfaces,” *IEEE Commun. Mag.*, vol. 59, no. 6, pp. 35–41, 2021.
- [8] P. Ramezani *et al.*, “Localization in massive MIMO networks: From far-field to near-field,” *Massive MIMO for Future Wireless Communication Systems: Technology and Applications*, pp. 123–150, 2025.
- [9] H. Lei *et al.*, “Near-field user localization and channel estimation for XL-MIMO systems: Fundamentals, recent advances, and outlooks,” *IEEE Wireless Commun.*, pp. 1–9, 2025.
- [10] D. Gürgünoğlu *et al.*, “Performance analysis of a 2D-MUSIC algorithm for parametric near-field channel estimation,” *IEEE Wireless Commun. Lett.*, vol. 14, no. 5, pp. 1496–1500, 2025.
- [11] P. Ramezani *et al.*, “An efficient modified MUSIC algorithm for RIS-assisted near-field localization,” in *Proc. IEEE Global Commun. Conf. (GLOBECOM)*, 2024.
- [12] I. Gavras *et al.*, “Near-field localization with 1-bit quantized hybrid A/D reception,” in *Proc. IEEE Int. Conf. Acoust., Speech, and Signal Process. (ICASSP)*, 2024.
- [13] X. Wei and L. Dai, “Channel estimation for extremely large-scale massive MIMO: Far-field, near-field, or hybrid-field?” *IEEE Commun. Lett.*, vol. 26, no. 1, pp. 177–181, 2022.
- [14] E. Björnson *et al.*, *Introduction to multiple antenna communications and reconfigurable surfaces*. Now Publishers, Inc., 2024.
- [15] J.-M. Conrat *et al.*, “Impact of rough building material surfaces on reflection coefficients from 5 GHz to 260 GHz,” in *Proc. Eur. Conf. Antennas and Propag. (EuCAP)*, 2025.
- [16] Y.-D. Huang and M. Barkat, “Near-field multiple source localization by passive sensor array,” *IEEE Trans. Antennas and Propag.*, vol. 39, no. 7, pp. 968–975, 1991.